Analysis of Large-Scale Phased Antenna Array With Generalized Transition Matrix

Shang Xiang, *Student Member, IEEE*, Gaobiao Xiao, *Member, IEEE*, Xuezhe Tian, *Student Member, IEEE*, and Junfa Mao, *Fellow, IEEE*

***Abstract*—This paper presents a numerical method to evaluate the electromagnetic radiating characteristics of a large-scale phased antenna array by using generalized transition matrix modules. Choosing an appropriate reference surface to contain an antenna element, an associated generalized transition matrix (GTM) is defined to establish the relationships between the rotated tangential components of incident field and scattered field on the reference surface. Meanwhile, a mapping vector is constructed to map the excitation sources onto the reference surface as the rotated tangential radiation field components. A GTM module for an antenna unit with feeding source consists of a GTM, a mapping vector, and a specified reference surface. The radiation pattern and mutual coupling effects among units can be analyzed by using the GTM modules of all units, in conjunction with the generalized surface integral equations (GSIEs). The interaction of the excitation port information is included in the field transmission process between the GTM modules as well. For a phased antenna array with fixed element structure and array size, the GTM modules and the coupling matrices among units do not change with the amplitude or phase of the feeding sources. The proposed method is particularly efficient to analyze the property of beam scanning and sidelobe level adjustment of a large-scale phased antenna array. Numerical results are provided to verify the high efficiency and precision of the method.**

***Index Terms*—Beam scanning, generalized transition matrix, mapping vector, phased antenna array, synthetic basis function.**

I. Introduction

As THE scale and complexity of modern electromagnetic system rise, effective and accurate computational methods to obtain the characteristics become particularly important. The traditional methods such as the method of moments (MOM) [1] cannot easily handle a multimodule system with sources such as the large phased antenna array because of the rapid growth of the computational complexity $(O(N^3))$ and memory cost $(O(N^2))$. Therefore, some flexible fast algorithms coupled with the MOM are proposed to overcome the difficulty. In these methods, only the near-field entries of the coupling matrix need to be stored, and the fast matrix-vector production in the iteration process is achieved by factorizing the Green's function. The most important one is the fast multiple method (FMM) [2] and its extension—the multilevel fast multipole algorithm (MLFMA) [3], [4]. This efficient matrix-vector production method is utilized by many other techniques such as the complex multipole beam approach (CMBA) [5], the impedance matrix localization (IML) technique [6], the adaptive method (AIM) [7], the multilevel matrix decomposition algorithm (MLMDA) [8], and the integral equation fast Fourier transform algorithm (IE-FFT) [9].

Other methods focus on reducing the number of unknowns without significant loss of the accuracy or on geometrical flexibility of the low-level basis functions. The concept of reducing the size of matrix equations is prevailing in recently developed iterative-free methods for large-scale problems, for instance, the characteristic basis function method (CBF) [10], the synthetic basis function approach (SBF) [11], the sub-entire-domain basis function method (SED) [12], the eigencurrent approach [13], and the subdomain multilevel approach [14]. The objectives of these methods are similar by employing macro basis functions for the surface electric and/or magnetic currents. The differences between these methods primarily arise from the way to generate the macro basis functions.

Meanwhile, recent development of domain decomposition method (DDM) [15]–[21] combined with the accelerating methods or further model order reduction methods mentioned above provides us a more efficient way to obtain field solution at each frequency point. When the DDM is applied, the system under consideration is divided into a lot of subdomains, and electromagnetic fields of each subdomain are solved independently. Then, the coupling effects of all subdomains are calculated to get the electromagnetic characteristics of the entire system.

In this paper, we implement the DDM with surface integral equation formulation based on the equivalence principle. We adopt the generalized transition matrix (GTM) algorithm [21] and make some important improvements to solve the subdomains with internal sources, such as antenna array units with feeding sources. In the GTM algorithm, the procedure to extract the scattering characteristics is similar to that in the equivalence principle algorithm (EPA) [18] and the linear embedding via Green's operators (LEGO) [20]. The scattering operators in both [18] and [20] are defined on the boundaries of domains that enclose complicated structures with fine details. However, the mutual mapping between the internal source and the boundary information is not dealt with in both EPA and LEGO methods, while it is proposed in this paper. In analysis of a large-scale phased antenna array with fixed structure but changing port excitations, the proposed method has distinct superiority. A reference surface is selected to define the subdomain containing an

Manuscript received February 22, 2013; revised August 08, 2013; accepted August 14, 2013. Date of publication August 22, 2013; date of current version October 28, 2013. This work was supported by the National Science Foundation of China under Grant 61234001 and the SAST 2013 Foundation.

The authors are with the Key Laboratory of Ministry of Education of Design and Electromagnetic Compatibility of High-Speed Electronic Systems, Shanghai Jiao Tong University, Shanghai 200240, China (e-mail: gaobiaoxiao@sjtu.edu.cn; jfmao@sjtu.edu.cn).

Digital Object Identifier 10.1109/TAP.2013.2279481

antenna element. The GTM module of the element consists of three parameters: the GTM representing the scattering property fabricated similarly as in [21], the mapping vector representing radiating property of the feeding, and the specified reference surface. The mapping vector is used to associate the internal voltage or current source with the rotated tangential radiation field components on the reference surface.

All subdomains are built in the same way. Their electromagnetic characteristics are evaluated independently by setting them in the background medium alone. The generalized surface integral equation (GSIE) [22] is used to combine the interactions of all units of the entire antenna array. SBFs [23] can be generated to further reduce the matrix dimension.

In many practical situations, the element structure in a phased antenna array, including the feeding structure in element, is identical, while the phase and magnitude of the feeding source varies with elements. If the reference surface is also selected to have identical geometry, then it is possible that all elements share a common GTM module and a common set of SBFs, perhaps with necessary coordinate translation and rotation operations.

The basic concept and construction of GTM module for single antenna element are described in Section II, while radiating problem of the antenna array utilizing the GSIE is discussed in Section III. The SBF extraction based on the GTM module and the modification of GSIE matrix are given in Section IV. Numerical examples for analysis of phased antenna arrays are provided in Section V.

II. Generating Procedure of GTM Module

Following the method described in [21], each antenna element is enclosed by a reference surface. The equivalent electric and magnetic current sources on the reference surface of a single antenna element come from two parts: One is produced by the induction effect of the superposition from all the other elements in the antenna array; the other is from the feeding sources within the element. The radiation field of the antenna element can be regarded to be generated by the equivalent electric and magnetic current sources obtained via the linear superposition of the two parts.

The reference surface and the excitation port can be regarded as two ports of the module. They are respectively called external port and internal port hereafter. In order to utilize the information on the external port to evaluate interaction between two elements, we need to map the internal port information onto the external port. Meanwhile, for the purpose of analyzing characteristics of the internal port under different interference or coupling signals imposed on the external port, the transmission path from external port to internal port should be built. It is also necessary to get the response property of the whole structure under external excitations, when the internal port is connected with a terminal load.

As shown in Fig. 1, an antenna element illuminating by exterior interference signals is bounded by a reference surface S. The element is located in the free space with the permittivity ε_0 and permeability μ_0. The reference surface can be selected as any arbitrary curved surface containing the target body.

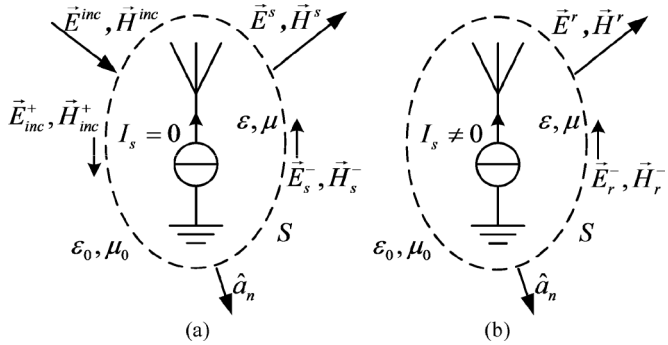

Fig. 1. (a) Antenna element with external incident field only as a scattering body. (b) Antenna element with internal feeding source only as a radiating body.

In Fig. 1(a), $\vec{E}^{\rm inc}, \vec{H}^{\rm inc}$ are incident fields illuminating on S and $\vec{E}^{S}, \vec{H}^{S}$ are resultant scattered fields aroused by equivalent sources on the reference surface. The rotated tangential filed components of the incident field and the scattered field on the reference surface S are denoted by

$$\boldsymbol{X}^{+} = \begin{bmatrix} \boldsymbol{E}^{+}_{\rm inc} \\ \boldsymbol{H}^{+}_{\rm inc} \end{bmatrix} = \left. \begin{bmatrix} \boldsymbol{E}^{\rm inc} \times \hat{a}_n \\ \hat{a}_n \times \boldsymbol{H}^{\rm inc} \end{bmatrix} \right|_S \tag{1}$$

$$\boldsymbol{X}^{-}_{s} = \begin{bmatrix} \boldsymbol{E}^{-}_{s} \\ \boldsymbol{H}^{-}_{s} \end{bmatrix} = \left. \begin{bmatrix} \boldsymbol{E}^{s} \times \hat{a}_n \\ \hat{a}_{\rm n} \times \boldsymbol{H}^{s} \end{bmatrix} \right|_S \tag{2}$$

where $\boldsymbol{X}^{+}$ and $\boldsymbol{X}^{-}_{s}$ are considered to be the "input signal" and "response signal" of the external port, respectively. The normal unit vector $\hat{a}_{\rm n}$ of the reference surface S points outward.

In Fig. 1(b), the antenna element works only under the current feeding source $I_{\rm s}$ without incident fields from exterior of the reference surface. The rotated tangential component of the radiation field $\vec{E}^{\rm r}, \vec{H}^{\rm r}$ aroused by the equivalent source generated from the feeding source is denoted by $\boldsymbol{X}^{-}_{\rm r}$ and defined as

$$\boldsymbol{X}^{-}_{\rm r} = \begin{bmatrix} \boldsymbol{E}^{-}_{\rm r} \\ \boldsymbol{H}^{-}_{\rm r} \end{bmatrix} = \left. \begin{bmatrix} \boldsymbol{E}^{\rm r} \times \hat{a}{\rm n} \\ \hat{a}{\rm n} \times \boldsymbol{H}^{\rm r} \end{bmatrix} \right|_S . \tag{3}$$

Taking both situations into account, we use linear superposition of the two kinds of responses from the external and internal signals. The final rotated tangential outgoing field components $\boldsymbol{X}^{-}$ on the reference surface S of a single antenna element are

$$\boldsymbol{X}^{-} = \boldsymbol{X}^{-}_{s} + \boldsymbol{X}^{-}_{\rm r} . \tag{4}$$

In practical situation, each element in a phased array is fed with a transmission line, whose characteristic impedance is equal to the system impedance, e.g., 50 Ω. A matching network is usually required to transform the system impedance to the input impedance of the element, which is denoted by Z_a, as shown in Fig. 2. Therefore, looking from the internal port, in a conjugate matched situation, the element is equivalent to being connected to an impedance $Z_{\rm in} = Z^{*}_{a}$. For the sake of simplicity, in the GTM module described in this paper, the matching network is not included. An element is matched means that the element is assumed to be connected to $Z_{\rm in} = Z^{*}_{a}$ directly.

In order to obtain the generalized transition matrix $\boldsymbol{T}$, the input impedance at the feeding port of the element has to be calculated first. Here, consider a simple case that the element consists of perfect electric conductor (PEC) and uniform media so

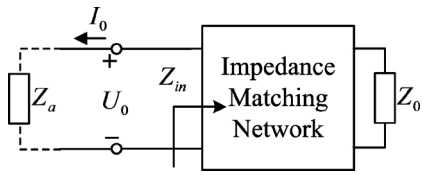

Fig. 2. Equivalent circuit model of the excitation port with terminal load.

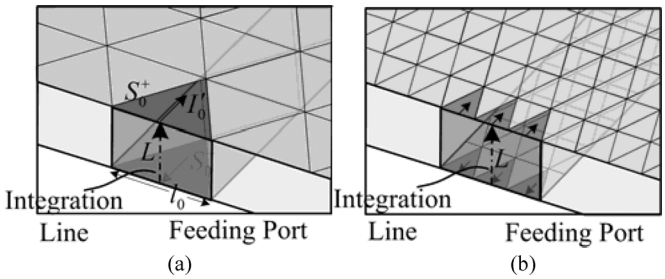

Fig. 3. Zoomed-in feeding port with special RWG basis function pairs. (a) Containing a single RWG basis. (b) Containing several RWG bases.

that the scattered or radiated fields can be determined by using surface integral equations with respect to surface electric/magnetic currents. It is also assumed that each element is fed at two points and the surface currents in the element are expanded with RWG basis functions $\vec{f}_n$. Fig. 3 shows the zoomed-in feeding port with meshes on the metal of the ground part and the feeding part. Two feeding points can be put within a special RWG basis $\vec{f}_0$, as shown in Fig. 3(a). Two triangles, S_0^+ located on the ground and S_0^- located on the feeding strip, constitute a normal RWG basis with its triangle pair being ripped apart by the excitation port, with one feeding point at one triangle and l_0 as its common edge.

When the size of the port is large, one single RWG basis is not enough to represent the port signal. Therefore, the special basis function $\vec{f}_0$ can be obtained by the aggregation of several RWG basis functions $\vec{f}_{0n}$ as drawn in Fig. 3(b)

$$\vec{f}_0 = \sum_{n=1}^{N_t} \beta_n \vec{f}_{0n} \tag{5}$$

where N_t is the number of the RWG basis function pairs included in $\vec{f}_0$. The coefficient vector $[\beta_1, \beta_2, \ldots, \beta_{N_t}]$ is the current distribution ratio determined by the inner product of $\vec{f}_{0n}$ and the rotated tangential components of the magnetic fields corresponding to the dominant transmission mode on the port.

In the following derivation, we set $N_e + 1$ basis functions on antenna element in total, of which one special basis function is for the port electric current and N_e are for the expansion of all the other electric and magnetic currents.

An imposed port electric current with coefficient I_0' shown in Fig. 3(a) is set on the special basis function with an open-circuited terminal. The distribution of electric and magnetic currents on the antenna elements under excitation of the feeding current can be solved by

$$\boldsymbol{Z} \cdot \boldsymbol{I} + \boldsymbol{K} I_0' = \boldsymbol{0} \tag{6}$$

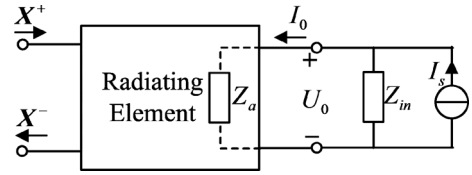

Fig. 4. Equivalent two-port circuit network model of an antenna element.

where $\boldsymbol{Z}$ is the $N_e \times N_e$ self-impedance matrix without consideration of the port special basis function and $\boldsymbol{K}$ is a $N_e \times 1$ column vector representing the test procedure on the fields generated by the port special basis function. The $N_e \times 1$ vector $\boldsymbol{I}$ stands for the currents on the antenna element (not including the imposed electric current).

The electric fields on the excitation port can be constructed by electric and magnetic currents including the feeding current with the dyadic Green function $\bar{\bar{G}}_0$ of the background medium as

$$\vec{E}^{\text{port}} = \int_S [-j\omega\mu_0 \bar{\bar{G}}_0 \cdot \vec{J} - \nabla \times \bar{\bar{G}}_0 \cdot \vec{M}] ds. \tag{7}$$

The port voltage is obtained by integrating the total electric fields along a predefined integration line shown in Fig. 3 as

$$U_0' = -\int_L \vec{E}_l \cdot d\vec{l} = \boldsymbol{F}^t \cdot \boldsymbol{I} + F' I_0' \tag{8}$$

where $\boldsymbol{F}$ is a $N_e \times 1$ column vector and the superscript t represents transposition. $F' = \int_L \hat{l} \cdot \int_S (j\omega\mu_0 \bar{\bar{G}}_0 \cdot \vec{f}_0) ds dl$, which is a scalar presenting the port voltage contributed by the port current I_0'.

Therefore, substituting (6) into (8), the input impedance of the antenna can be calculated by

$$Z_a = \frac{U_0'}{I_0'} = -\boldsymbol{F}^t \cdot \boldsymbol{Z}^{-1} \cdot \boldsymbol{K} + F'. \tag{9}$$

The antenna element with a specified reference surface can be modeled as a generalized two-port circuit network shown in Fig. 4. We aim to obtain the characteristic parameters of the network by building the relationship between signals of the two ports.

In a practical situation, an antenna element is usually illuminated by external incident fields, so the currents on the antenna element should be solved as

$$\boldsymbol{Z} \cdot \boldsymbol{I} + \boldsymbol{K} I_0 = \boldsymbol{D}_{\text{in}} \cdot \boldsymbol{X}^+ \tag{10}$$

where I_0 is the coefficient of the induced electric current on the port. Assuming there are N_g unknowns on the reference surface, $\boldsymbol{D}_{\text{in}}$ is a $N_e \times N_g$ matrix, representing field propagation from the reference surface to the antenna unit as defined in [21]. Again, the matrix equation (10) is derived by testing the corresponding integral equations on all basis functions except the special basis function for the internal port. (8), is applied to calculate the port voltage U_0, where I_0' is replaced by I_0, so we can rewrite it as

$$\boldsymbol{F}^t \cdot \boldsymbol{I} + F' I_0 = U_0. \tag{11}$$

The rotated tangential outgoing field components on the reference surface can be obtained as

$$\boldsymbol{X}^{-} = \boldsymbol{D}_{\text{out}} \cdot \boldsymbol{I} + \boldsymbol{D}_0 I_0. \tag{12}$$

The $N_{\text{g}} \times N_{\text{e}}$ matrix $\boldsymbol{D}_{\text{out}}$ is the same as that defined in [21] and [24], representing the mapping process from the rest electric and magnetic currents onto the reference surface in the form of rotated tangential components. The column vector $\boldsymbol{D}_0$ maps the electric fields and magnetic fields created by the port electric current onto the reference surface. $\boldsymbol{D}_{\text{out}}$ and $\boldsymbol{D}_0$ are calculated by testing on the reference surface the rotated tangential components of the outgoing fields that scattered by the equivalent currents $\boldsymbol{I}$ in the antenna element and the current I_0 on the special basis, respectively.

Substituting (10) into (12) to eliminate $\boldsymbol{I}$, the outgoing rotated tangential components can be expressed as

$$\boldsymbol{X}^{-} = \boldsymbol{D}_{\text{out}} \boldsymbol{Z}^{-1} \cdot (\boldsymbol{D}_{\text{in}} \cdot \boldsymbol{X}^{+} - \boldsymbol{K} I_0) + \boldsymbol{D}_0 I_0. \tag{13}$$

Similarly, substituting (10) into (11), the port voltage is obtained as follows:

$$U_0 = \boldsymbol{F}^t \cdot \boldsymbol{Z}^{-1} \boldsymbol{D}_{\text{in}} \cdot \boldsymbol{X}^{+} - \boldsymbol{F}^t \cdot \boldsymbol{Z}^{-1} \cdot \boldsymbol{K} I_0 + F' I_0. \tag{14}$$

Combining with the input impedance of the antenna calculated in (9), (14) can be updated as

$$U_0 = \boldsymbol{F}^t \cdot \boldsymbol{Z}^{-1} \boldsymbol{D}_{\text{in}} \cdot \boldsymbol{X}^{+} + Z_a I_0. \tag{15}$$

Now the parameters of the equivalent two-port network in Fig. 4 can be derived as

$$\begin{bmatrix} \boldsymbol{X}^{-} \\ U_0 \end{bmatrix} = \begin{bmatrix} \boldsymbol{A} & \boldsymbol{M} \\ \boldsymbol{C}^t & Z_a \end{bmatrix} \begin{bmatrix} \boldsymbol{X}^{+} \\ I_0 \end{bmatrix} \tag{16}$$

where

$$\begin{aligned} \boldsymbol{A} &= \boldsymbol{D}_{\text{out}} \boldsymbol{Z}^{-1} \boldsymbol{D}_{\text{in}} \\ \boldsymbol{M} &= (\boldsymbol{D}_0 - \boldsymbol{D}_{\text{out}} \boldsymbol{Z}^{-1} \cdot \boldsymbol{K}) \\ \boldsymbol{C}^t &= \boldsymbol{F}^t \cdot \boldsymbol{Z}^{-1} \boldsymbol{D}_{\text{in}}. \end{aligned}$$

Apparently, the incident fields on the reference surface will generate a scattered fields on the external port and a coupling signal on the internal port.

According to Fig. 4, the port voltage and current satisfy the following equation:

$$U_0 = Z_{\text{in}}(I_{\text{s}} - I_0) \tag{17}$$

where I_{s} is the current of the excitation source. Substituting (17) into (15), the relationship between the port current and excitation source current under external incident fields can be established as

$$I_0 - \frac{Z_{\text{in}}}{Z_a + Z_{\text{in}}} I_{\text{s}} = \frac{-\boldsymbol{F}^t \cdot \boldsymbol{Z}^{-1} \boldsymbol{D}_{\text{in}}}{Z_a + Z_{\text{in}}} \boldsymbol{X}^{+}. \tag{18}$$

Substituting (18) into (13) yields the rotated tangential component of the outgoing field on the reference surface

$$\boldsymbol{X}^{-} = \left(\boldsymbol{A} - \frac{\boldsymbol{M} C^t}{Z_a + Z_{\text{in}}} \right) \cdot \boldsymbol{X}^{+} + \boldsymbol{M} \frac{Z_{\text{in}}}{Z_a + Z_{\text{in}}} I_{\text{s}} \tag{19}$$

where $\boldsymbol{M}C^t$ is a dyadic. The GTM is defined as

$$\boldsymbol{T} = \boldsymbol{A} - \frac{\boldsymbol{M} C^t}{Z_a + Z_{\text{in}}} \tag{20}$$

which connects the rotational components of the scattered field and the incident field on the reference surface S directly. The column vector $\boldsymbol{M}$ in (19) is defined as the mapping vector. For elements with multiple feeding sources, I_{s} becomes a vector, and $\boldsymbol{M}$ becomes a matrix.

It can be checked that the parameters of the two-port network model—namely, $\boldsymbol{A}$, $\boldsymbol{M}$, and $\boldsymbol{C}$ in (16)—are all independent upon excitations and terminal load. However, the GTM defined in (20) is dependent on the load impedance Z_{in}. When the antenna element is terminated by a matched load, the GTM is denoted as

$$\tilde{\boldsymbol{T}} = \boldsymbol{A} - \frac{\boldsymbol{M} C^t}{2R_a} \tag{21}$$

where R_a is the resistance of complex impedance Z_a. In order to verify the physical meaning of the model, (19) is reorganized as

$$\boldsymbol{X}^{-} = \left(\boldsymbol{A} - \frac{\boldsymbol{M} C^t}{2R_a} + s \frac{\boldsymbol{M} C^t}{2R_a} \right) \cdot \boldsymbol{X}^{+} + \boldsymbol{M} \frac{Z_{\text{in}}}{Z_a + Z_{\text{in}}} I_{\text{s}} \tag{22}$$

where s equals to $(Z_{\text{in}} - Z_a^*)/(Z_{\text{in}} + Z_a)$, which is defined as the power wave reflection coefficient proposed in [25]. It is possible that an element in a phased array is not fed but simply connected to an impedance load. When the load is power unmatched, a reflected current I_{r} appears on the internal port, which will generate radiation fields exactly like a feeding current. In the case that there is no feeding source current I_{s}, the total port electric current with unmatched terminal is the superposition of the induced port electric current $\tilde{I}_0$ with conjugate matched terminal and the reflected electric current I_{r} with unmatched power load, which can be written as

$$I_0 = \tilde{I}_0 + I_{\text{r}} = \tilde{I}_0 (1 - s). \tag{23}$$

The port induced electric current $\tilde{I}_0$ with matched terminal is calculated as

$$\tilde{I}_0 = -\frac{\boldsymbol{C}^t}{2R_a} \cdot \boldsymbol{X}^{+}. \tag{24}$$

According to (21), (23), and (24), (22) can be transformed to

$$\boldsymbol{X}^{-} = \tilde{\boldsymbol{T}} \cdot \boldsymbol{X}^{+} + \boldsymbol{M} \left(I_{\text{r}} + \frac{Z_{\text{in}}}{Z_a + Z_{\text{in}}} I_{\text{s}} \right). \tag{25}$$

The scattering characteristics of an antenna element can be described by $\tilde{\boldsymbol{T}}$, the GTM with matched load. As long as the antenna structure is fixed, $\tilde{\boldsymbol{T}}$ does not change with the terminal load. The second term in right-hand side of (25) shows the mapping from the shunted source current and the reflected current onto the reference surface. The two kinds of currents share the same mapping vector $\boldsymbol{M}$. In practical cases, the reflected current I_{r} shows the effect of different terminal loads.

The physical meaning of the module can be explained by the two-port network model. The characteristics of each antenna element in the array can be accessed accurately by the GTM module without consideration of the internal complex structure.

In general, we try to design an antenna with a matched terminal in order to improve the radiation performance, so usually the GTM module with $\tilde{\boldsymbol{T}}$ in matched situation is all we need to construct. In practical situation, slightly unmatched terminal load does not affect much accuracy of the results applying the matched GTM module.

Although it is a little complex and time-consuming to construct the GTM module of one antenna element than to solve the MOM matrix equations straightly, the advantage occurs when solving problems of the phased antenna array or multimodules system. While analyzing independent element of the antenna array, the scattering and radiating characteristics can be completely extracted by the GTM and the mapping vector, respectively. Modules with different internal elements can be generated applying parallel algorithm to enhance the whole efficiency to solve a large multimodules system due to the characteristics of the modules are independent with each other.

III. GSIE Solution

After the GTM module is obtained, the GSIE is established as a new linear system containing the coupling information between the elements to solve the general radiation field of the array system. As the dimension of the GTM module is decided by the number of basis functions on the reference surface, the dimension of the new linear system established by the GTM module is much less than the traditional MOM matrix equations, which greatly enhance the efficiency of solving large-scale array.

Considering the multiradiating structure shown in Fig. 5, we separate the array system to M elements according to its natural boundary. Each element is surrounded by its reference surface where the GTM module has been built. The information of the mth element participating interaction with the others is only conveyed by the calculated GTM module with the GTM $\boldsymbol{T}_m$ and the mapping vector $\boldsymbol{M}_m$. The rotated tangential outgoing field components of block-n on the reference surface are supposed as $\boldsymbol{X}_n^-$, by which the outgoing fields anywhere in the space can be calculated using the fundamental integral equations. Through the field transmission between modules, the outgoing fields of the block-n become part of the excitation fields on the other modules. The total incident fields are the superposition of the outgoing fields from all the other modules in the array, which we can apply to establish the iterative equations.

The outgoing fields from the reference surface S_n of block-n will travel to reference surface S_m of block-m, and their rotated tangential components become the "incident fields" of block-m. This wave transmission process can be described as

$$\boldsymbol{X}_{m,n}^+ = \boldsymbol{D}_{m,n} \cdot \boldsymbol{X}_n^- \tag{26}$$

where $\boldsymbol{D}_{m,n}$ is defined as the field transmission matrix from block-n to block-m, which is not necessary to be a square matrix because the dimensions of the two blocks may be not the same. All the entries in matrix $\boldsymbol{D}_{mn}$ are evaluated with double surface integrals, which can be found in [22].

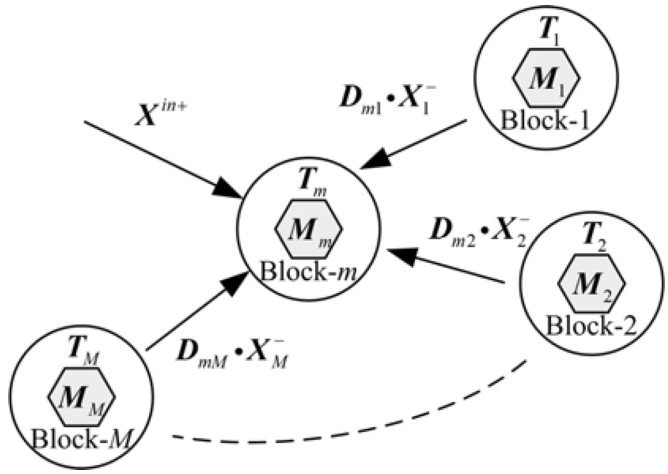

Fig. 5. Incident fields on block-m from all the other blocks.

Taking block-m as the target as shown in Fig. 5 and combining with (26), the total incident field on reference surface S_m is defined as

$$\boldsymbol{X}_m^+ = \sum_{n=1, n\neq m}^{M} \boldsymbol{D}_{m,n} \cdot \boldsymbol{X}_n^- + \boldsymbol{X}_m^{\mathrm{in}+}. \tag{27}$$

$\boldsymbol{X}_m^{\mathrm{in}+}$ is the rotated tangential components of the external interference excitation field that needs to be considered only when the electromagnetic system exposed in the external interference fields.

Substituting (27) into (19) yields

$$\boldsymbol{X}_m^- = \boldsymbol{T}_m \cdot \left(\sum_{n=1, m\neq n}^{M} \boldsymbol{D}_{m,n} \cdot \boldsymbol{X}_n^- \right) + \boldsymbol{M}_m I_m + \boldsymbol{T}_m \cdot \boldsymbol{X}_m^{\mathrm{in}+} \tag{28}$$

where I_m equals to $(Z_{\mathrm{in}}^{(m)}/(Z_a^{(m)} + Z_{\mathrm{in}}^{(m)}))I_{\mathrm{s},m}$. This formula is the discretized form of generalized surface integral equation on reference surface S_m. By solving this linear system, we can get the total outgoing field tangential component on each reference surface of the antenna elements in order to solve the far-field radiation of the array. For the antenna array, the order of the GSIE can be much less than that of traditional MOM so the method will significantly reduce the number of unknowns.

IV. SBF Implementation on GSIE

The application of the SBFs on GSIE can extract some most important characteristics in order to further reduce the system scale and improve the solving efficiency of the system without

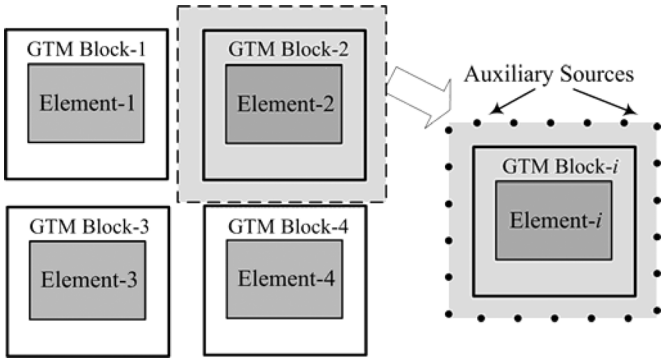

Fig. 6. Auxiliary sources displacement on a decomposed block of the GTM module in an array.

loss of the accuracy. To achieve such goal of information compression, two important processes are introduced in generating SBFs on the blocks: 1) adopting equivalent auxiliary sources to obtain the solution spaces; and 2) applying singular value decomposition (SVD) to generate characteristic vectors.

As to the antenna array analysis based on the GTM module domain decomposition, we choose one of the blocks to analyze and establish an independent model as shown in Fig. 6. This block is surrounded by series of auxiliary sources with man-made definition. The auxiliary sources are set as external excitations from all different directions to the GTM block. In Fig. 6, we employ the cubical virtual surface irregularly meshed into triangle patches as the method in [24].

Assuming that we have defined $N_{\rm s}$ auxiliary sources for the mth block, an external solution space is generated to embody the scattering characteristics as

$$\boldsymbol{R}_m^{(1)} = \left[\tilde{\boldsymbol{T}}_m \cdot \boldsymbol{X}_{1,m}^{\rm ex+}, \tilde{\boldsymbol{T}}_m \cdot \boldsymbol{X}_{2,m}^{\rm ex+}, \ldots, \tilde{\boldsymbol{T}}_m \cdot \boldsymbol{X}_{N_{\rm s},m}^{\rm ex+}\right] \tag{29}$$

where $\boldsymbol{X}_{k,m}^{\rm ex+}$ is the incident field from the kth auxiliary source. If there are $N_{\rm f}$ internal sources inside the block, the other solution space embodying the radiating characteristics can be generated in form of

$$\boldsymbol{R}_m^{(2)} = \left[\boldsymbol{M}_{1,m} I_{1,m}, \boldsymbol{M}_{2,m} I_{2,m}, \ldots, \boldsymbol{M}_{N_{\rm f},m} I_{N_{\rm f},m}\right]. \tag{30}$$

The SVD process is applied to extract the independent vectors of the two solution spaces separately as the method in [23]. If only one internal source exists in the block, it is not necessary to perform SVD on the solution space $\boldsymbol{R}_m^{(2)}$, and the mapping vector can be used as SBF for this solution space directly.

According to (25), even if the array element connects to an unmatched load, the two solution spaces are not necessary to be changed because the reflected current and the feeding current exist simultaneously at the same position of the antenna. For an antenna units with fixed structures, the GTM modules share one set of SBFs no matter whether the terminal is matched or not.

We denote the kth SBF of the mth element as

$$\vec{F}_k^{(m)} = \sum_{i=1}^{N_{\rm g}} a_{i,k}^{(m)} \vec{f}_i^{(m)}, \qquad k = 1, 2, \ldots, K \tag{31}$$

where the SBF $\vec{F}_{m,k}$ is an aggregation of the lower-order basis functions $\vec{f}_i^{(m)}$ on the reference surface, and $a_{i,k}^{(m)}$ is the kth column vector of the singular matrix obtained by SVD. The columns after the Kth column can be claimed as no longer independent if the ratio of the $(K+1)$th column is smaller than the threshold we set. The first K columns are chosen as the coefficients to construct SBFs of block-m. For antenna array with the same construction, the SBFs on each module can be set as the same, and the SBF vectors on block-m are represented by

$$\boldsymbol{\alpha}^{(m)} = \left[\boldsymbol{\alpha}_1^{(m)}, \boldsymbol{\alpha}_2^{(m)}, \ldots, \boldsymbol{\alpha}_K^{(m)}\right], \qquad m = 1, 2, \ldots M. \tag{32}$$

The undetermined field tangential components on the reference surface can be replaced by expansion of the synthetic basis functions

$$\boldsymbol{X}_m^- = \sum_{k=1}^{K} \varphi_k^{(m)} \vec{F}_k^{(m)}. \tag{33}$$

Substituting (33) into (28) yields

$$\sum_{n=1}^{M} \boldsymbol{P}^{(m,n)} \cdot \boldsymbol{\varphi}^{(n)} = \left(\boldsymbol{\alpha}^{(m)}\right)^t \cdot \boldsymbol{M}_m I_m + \left(\boldsymbol{\alpha}^{(m)}\right)^t \cdot \boldsymbol{T}_m \cdot \boldsymbol{X}_m^{\rm in+} \qquad m = 1, 2, \ldots M. \tag{34}$$

The entries of the size-reduced coefficient matrix $\boldsymbol{P}$ can be constructed considering the self and mutual coupling effect as

$$\boldsymbol{P}^{(m,n)} = \begin{cases} \left(\boldsymbol{\alpha}^{(m)}\right)^t \cdot \boldsymbol{\alpha}^{(n)}, & m = n \\ -\left(\boldsymbol{\alpha}^{(m)}\right)^t \cdot \boldsymbol{T}_m \boldsymbol{D}_{m,n} \cdot \boldsymbol{\alpha}^{(n)}, & m \neq n. \end{cases} \tag{35}$$

Substituting the results of (34) into (33), the rotated tangential components of the radiation field can be obtained. In addition, if the whole structure of the array keeps invariant, the $\boldsymbol{P}$ matrix stays constant, which needs to be calculated only once and can be reutilized with the change of feeding signal and the environment excitation. If some elements in the array adjust their positions, we just need to recalculate the field transmission matrices related with these elements to modify the coupling matrix.

Through establishing reasonable threshold value, a small amount of SBFs can effectively indicate the characteristics of a GTM module. Usually the number of SBFs is far less than that of basis function on the reference surface and the order of the final matrix is further reduced. The number of SBFs is controllable, enabling us to make a compromise between the precision and the efficiency when analyzing the large-scale phased arrays.

V. Numerical Results

In this section, a practical Vivaldi antenna array is analyzed to verify the high efficiency and precision of the proposed method. At first, we discuss the results of a single element compared to traditional methods and the isolation degree compared to business software. Then, a large-scale phased array is considered to validate the feasibility and superiority for such application.

A. Single GTM Module

Referring to Fig. 7, the geometry size of a Vivaldi antenna is listed as follows: $W = 9$ cm, $W_{\rm t} = 7$ cm, $W_{\rm s} = 0.3$ cm, $W_{\rm k} = 0.2$ cm, $L = 18$ cm, $L_{\rm t} = 8.5$ cm, $L_{\rm s} = 0.3$ cm,

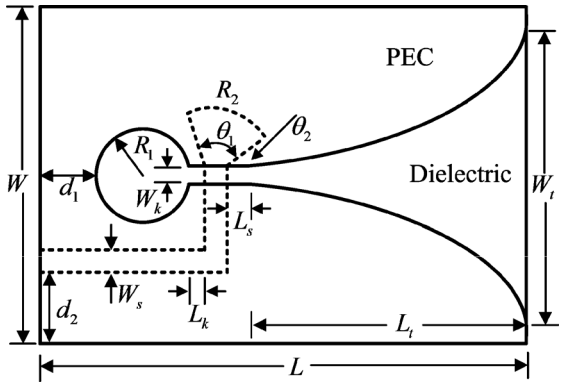

Fig. 7. Geometry parameters of a single Vivaldi array element.

$d_1 = 0.7$ cm, $d_2 = 2$ cm, $R_1 = 1$ cm, $R_2 = 1.5$ cm, $\theta_1 = 77°, \theta_2 = 31°$. The substrate relative dielectric constant $\varepsilon_{\rm r}$ is 2.2, and thickness t is 0.4 cm. A typical spatial sampling rate of $\lambda/10$ is usually required in the conventional implementation of MOM for discretization. Based on the criterion, the element is meshed by 1593, 449, and 50 RWG basis functions on the dielectric, the ground, and the feedline respectively. The center work frequency of the antenna is 2.4 GHz.

The GTM reference surface set close to the antenna element is meshed by 512 RWG basis functions. The radiation patterns calculated by both MOM and the GTM module for a single antenna element at 2.4 GHz are compared in Fig. 8.

In both E-plane and H-plane, the results of the GTM module match well with those of the reference MOM over the entire angular spectrum, which validates that the characteristics extraction by the GTM module is accurate and feasible. The time consumption and the unknown numbers are shown in Table I. Although the time of constructing GTM module is longer than the MOM method, the unknown number can be greatly reduced.

Then, by setting a threshold of singular value ratio as 0.02, 18 SBFs are chosen after SVD process to further reduce the unknown number of a single element. The singular value ratio versus the number of SBFs of a single element is plotted in Fig. 9. The accuracy of the SBF extracted on GTM with respect to that obtained by rigorous MOM algorithm is represented by the relative errors of radiation field in E-plane calculated by the two methods

$$\mathrm{Err} = \left(\sum_{i=1}^{360} |rE_{\rm SBF}(\varphi_i) - rE_{\rm MoM}(\varphi_i)|^2 \Big/ \sum_{i=1}^{360} |rE_{\rm MoM}(\varphi_i)|^2 \right)^{0.5} \times 100\% \quad (36)$$

where $\varphi_i = i\pi/360,\ i = 1, 2, \ldots, 360$. The curve of Err versus SBF number is also plotted in Fig. 9. The relative error of the radiation field calculated by 18 SBFs chosen as in Table I is below 0.3%, which is in an acceptable range. The determination of the unknown number needs to meet the demand of precision and order reduction.

B. Port Mutual Coupling

The schematic of mutual coupling of two antenna elements is shown in Fig. 10. The antenna input impedance $Z_{\rm a}$ has been

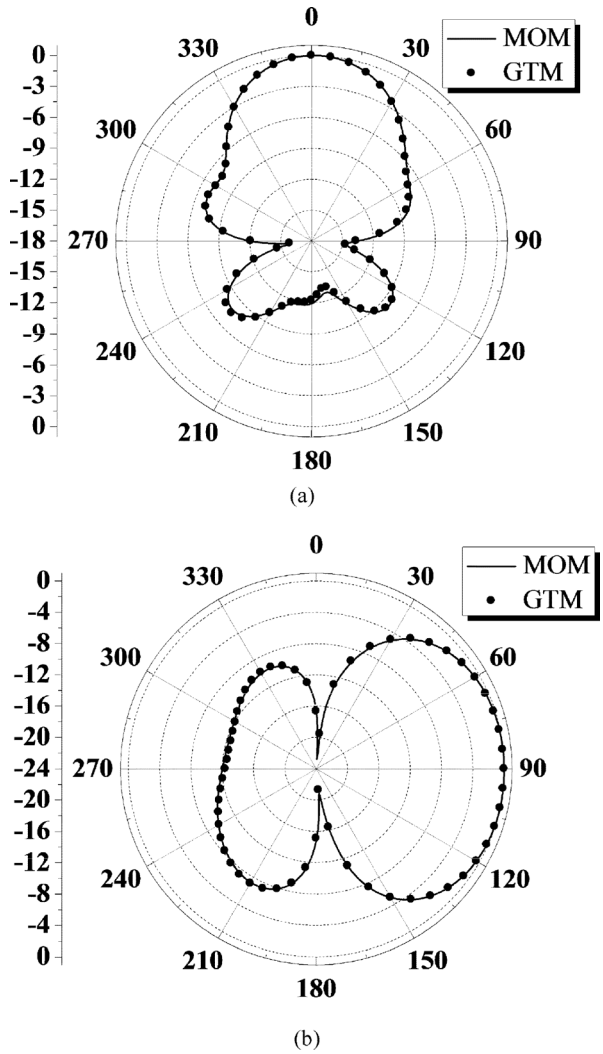

Fig. 8. Radiation patterns in (a) E-plane and (b) H-plane of a single antenna element.

TABLE I
CONSTRUCTION STATISTICS FOR SINGLE ELEMENT

Method	Time for each step	Total time	Number of Unknowns
MOM	240s	240s	3685
GTM	430s	670s	1024
SBF + GTM	145s	815s	18

calculated in (9) during the process of constructing the GTM module. The antenna element in block-1 is fed by an electric source $I_{\rm s}$, and the element in block-2 is terminated by a matched load. According to the GSIE, the incident and outgoing fields components on the reference surface can be obtained. Then, (16) is applied to solve the voltage and current on each internal port of the two blocks. Thus the mutual coupling of the two excitation ports can be calculated.

To demonstrate the ability of the GTM module in analyzing mutual coupling of antenna feeding ports, the port isolation of two elements with distance of 0.125 m is calculated as shown in Fig. 11. The maximum error compared to business software is less than 1.5 dB. Both the antenna element and the GTM

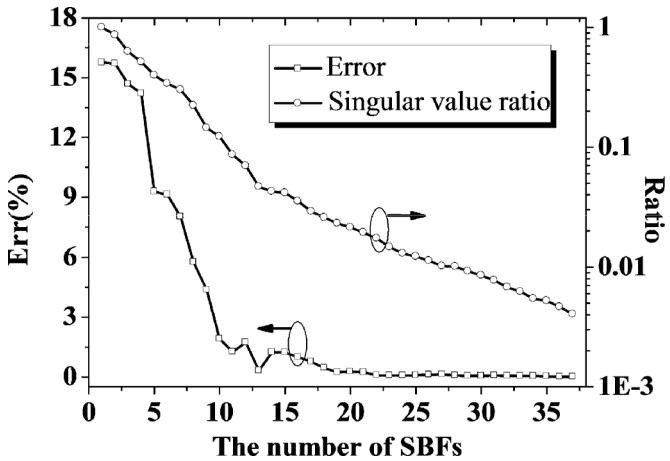

Fig. 9. Choice of the number of SBFs for a single element. Line with empty square: the relative error in E-plane. Line with empty circle: the singular value ratio versus the number of SBFs on single block.

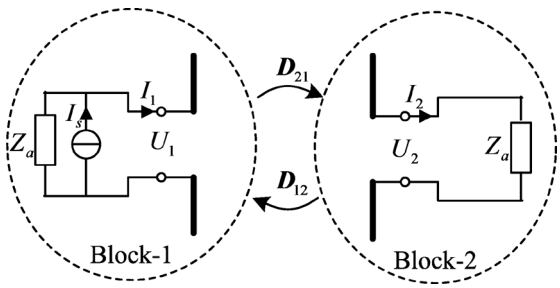

Fig. 10. Schematic of mutual coupling of two antenna elements.

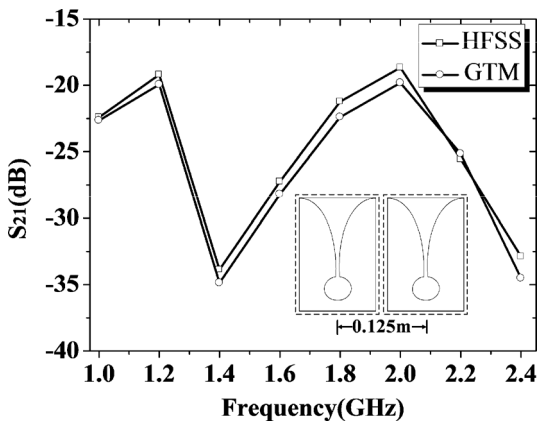

Fig. 11. Isolation degree of two Vivaldi antenna elements.

reference surface are chosen to be meshed based on the highest interested frequency.

In large antenna array, the information on the ports of different blocks is transmitted by coupling effect between GTM modules instead of direct interaction between antenna elements. Therefore, the efficiency is improved, especially in analyzing ports coupling of elements in large-scaled array. Meanwhile, the method can be applied to analyze the port responses under the external noise and to predict the antenna RCS reduction precisely.

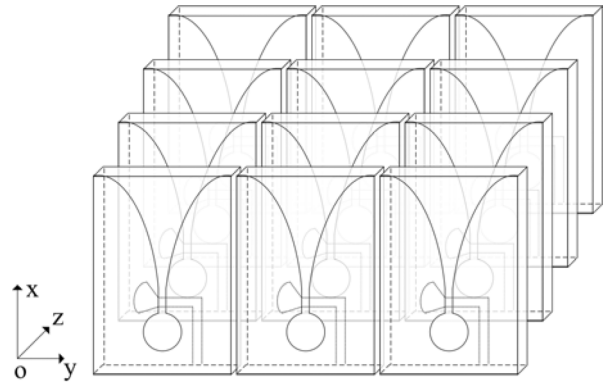

Fig. 12. Geometry of a finite $N \times M$ Vivaldi antenna array.

C. Large-Scale Phase Antenna Array

In general, assuming there are M elements in an antenna array, the GSIE matrix includes $M \times (M-1)$ field transmission matrices. However, for the periodic antenna array with P elements in row and Q elements in column, the $PQ \times (PQ-1)$ field transmission matrices contain a lot of same elements since arbitrary two pairs of the GTM blocks with the same relative displacement have the same value, which can be expressed as

$$\boldsymbol{D}_{i,j} = \boldsymbol{D}_{p,q} \quad \vec{r}_i - \vec{r}_j = \vec{r}_p - \vec{r}_q. \tag{37}$$

The transmission matrix is only determined by the relative coordinate position of the two blocks. As long as the condition satisfies, it can be called repeatedly after being calculated once. For example, there are 72 field transmission matrices of the 3×3 period array, but only 24 of which are different from each other. By summarizing the rules, we get the conclusion that $2 \times (2PQ - P - Q)$ different transmission matrices need to be calculated at least.

As the array size rises, the saved time for repeated calculations becomes considerable. For instance, the whole number of the transmission matrices of a 10×10 period array is 27.5 times as many as the number of transmission matrices with different values.

A sample example is shown in Fig. 12, where an $N \times M$ Vivaldi antenna array is plotted and all elements are operated at frequency $f = 2.4$ GHz with the structure size and mesh as shown in Fig. 7. The distance in the z- and y-directions between two adjacent elements is 5.8 and 10 cm, respectively. The computational results are shown in Table II for various array sizes, ranging from a 2×2 up to 20×20 elements. The unknown number for elements is determined by preprocessed single element as listed in Table I. When the array scale reaches 8×8, the system requires more than 200 000 unknowns for traditional MOM, the direct solution of which is beyond the ability of our PC. Even so, the proposed method shows its advantage in computational efficiency obviously when there are more than four elements in the array according to the comparison of the achievable CPU time between the proposed method and conventional MOM in Table II. The relative error calculated by (36) keeps below 1% within a reasonable tolerance applying the proposed method.

TABLE II
COMPUTATION RESULTS OF THE ANTENNA ARRAY

Size	RWG Number of MOM	RWG Number of GTM	SBF Number	D matrix* Number	Total CPU Time with proposed method (min.)	Total CPU Time with traditional MOM (min.)
2×2	15580	4096	72	8	16.3	57.37
4×4	62320	16384	288	48	31.85	892.19
6×6	140220	36864	648	120	60.98	18581.1
8×8	249280	65536	1152	224	102.1	-
10×10	389500	102400	1800	360	174.6	-
12×12	560880	147456	2592	528	253.44	-
14×14	763420	200704	3528	728	348.3	-
16×16	997120	262144	4608	960	470.8	-
18×18	1261980	331776	5832	1224	622.52	-
20×20	1558000	409600	7200	1520	819.91	-

*: Field transmission matrices needed to be calculated at least

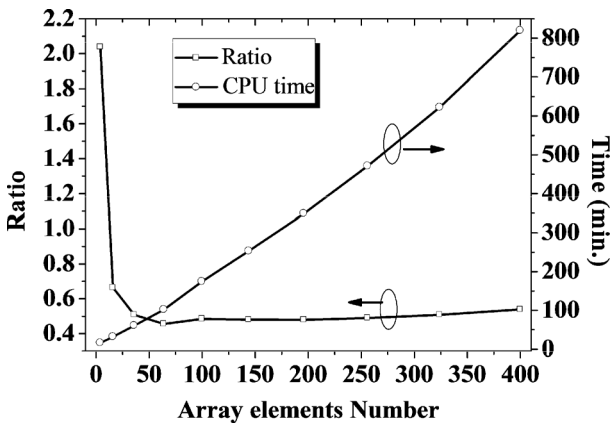

Fig. 13. Total CPU time to calculate the array and the ratio of the total time to the minimum number of the D matrix.

In order to show more clearly, the total CPU time with proposed method in Table II is illustrated in Fig. 13. The total CPU time contains the time cost in constructing the GTM module, extracting the SBFs, constructing the coupling $\boldsymbol{P}$ matrix, and solving the final equation system, not including the calculation time in solving the system under different feeding combinations. As expected, the CPU time increases linearly with the rising number of the array elements. According to the ratio of the total CPU time to the minimum number of the $\boldsymbol{D}$ matrix shown in Table II, we find that the primary reason for the consumption of computational time changes with the scale of the array. When the array size is small enough, the construction of the GTM module and the SBF extraction procedure consume most of the time. In the procedure to solve the middle-sized array, the construction of $\boldsymbol{P}$ matrix plays a dominant role, so the ratio curve keeps almost constant. Nevertheless, as the order of the $\boldsymbol{P}$ matrix rises, the matrix solving procedure will certainly spend more time. After the SVD procedure, only 18 SBFs for one GTM module of the period array are retained to represent the module characteristics.

The GTM module and the SBF are not necessary to recalculate with the change of the feed phase and magnitude as long as the element structure and the feed position stay the same. The module coupling $\boldsymbol{P}$ matrix does not change with fixed element structure and array size. The order of $\boldsymbol{P}$ matrix in (34) decided by the number of the SBFs has been decreased to an acceptable size as shown in Table II.

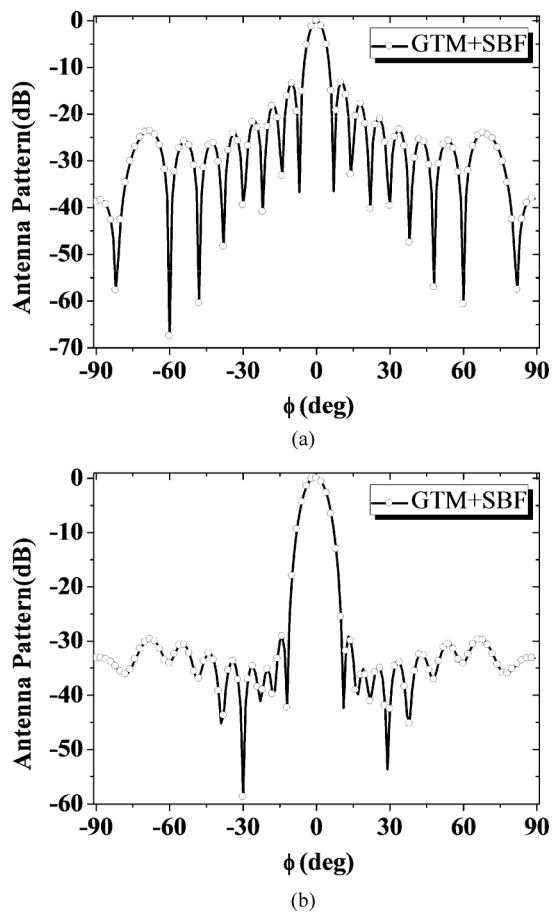

Fig. 14. Antenna patterns in E-plane of the 10×10 period Vivaldi broadside array ($\theta = 90°$). (a) With uniform feed magnitude. (b) With Chebyshev synthesis feed magnitude.

Taking the 10×10 phased array as an example, we assume that the beam scanning angle varies from 0° to $(N-1)°$, so N results are required if the designer needs predict the array performance of each angle. For N different feeding ways of the array, the coupling matrix only needs to be calculated only once. With the invariance of the $\boldsymbol{P}$ matrix in the proposed method, each result can be obtained within 2 min by modifying the feeding information and solving the stored $\boldsymbol{P}$ matrix without reconstruction. The saved time is quite considerable and the enhancement of efficiency is significant. Examples with the variation of feeding magnitude and phase are presented below.

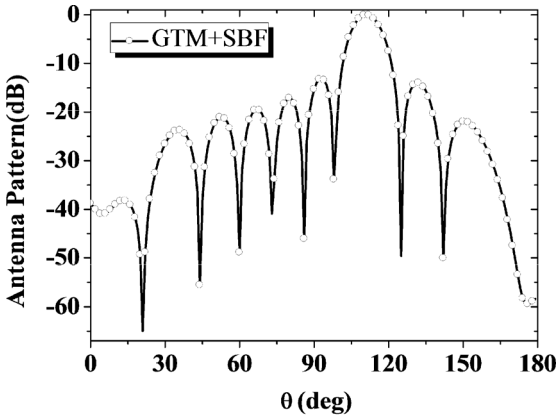

(a)

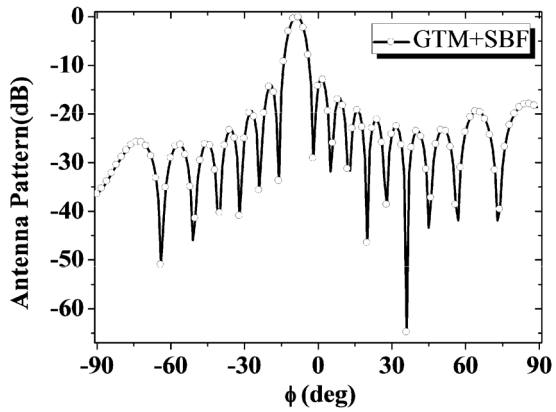

(b)

Fig. 15. Antenna patterns in (a) H-plane of the 10×10 Vivaldi period array with 60° phase variation in zz-direction ($\phi = 0^\circ$) and (b) E-plane of the 10×10 Vivaldi period array with 45° phase variation in y-direction ($\theta = 90^\circ$).

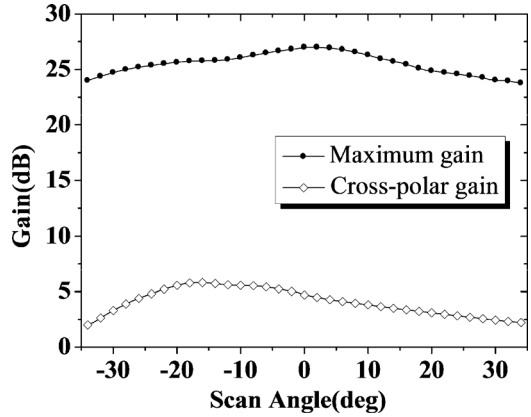

Fig. 16. Gain and cross-polar gain of the 10×10 Vivaldi array in beam scanning direction with scan angle from -35° to 35° in E-plane.

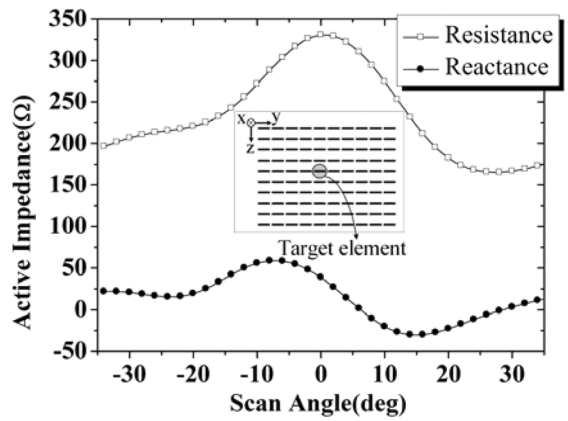

Fig. 17. Active impedance of the target element in the 10×10 Vivaldi array with scan angle in E-plane.

In order to obtain the low sidelobe and high pointing accuracy, the Chebyshev synthesis is used with -30 dB sidelobe level (SLL). According to [26], for the 10×10 array, the distribution of the Chebyshev incentive amplitude of each element in y-direction is 1: 1.6695: 2.5986: 3.4095: 3.883: 3.883: 3.4095: 2.5986: 1.6695: 1. The E-plane radiation pattern with Chebyshev synthesis feed plotted in Fig. 14(b) has obvious improvement compared to the result with uniform feed magnitude in Fig. 14(a). Please note that the array plane is parallel to the yoz-plane, as shown in Fig. 12. θ is the polar angle with respect to z-axis, and ϕ is the azimuth angle.

In analyzing the property of the beam scanning, the efficiency is also greatly improved without reconstructing the $\boldsymbol{P}$ matrix, which is independent with the diverse phases. The examples of the 10×10 phased array with the phase of the feeding signals varying respectively in z-direction and in y-direction are plotted in Fig. 15.

Fig. 16 shows the gain and cross-polar gain of the 10×10 phased array in beam-scanning direction in E-plane. The maximum scan loss in the process of scanning is less than 3 dB. From -35° to 35° of the scan angle, the cross-polar gain is about 21 dB lower than the total gain. The array has a good rejection on the cross polarization.

It is also an advantage of the proposed method to calculate the active impedance of the array elements. The rotated tangential components of the outgoing fields on all the GTM blocks under different feeding combinations can be quickly obtained after the $\boldsymbol{P}$ matrix is constructed. The coupling fields by all the other elements can be readily obtained. According to the two-port network model introduced in Section II, we utilize the GTM module to transmit the coupling signal from the reference surface of the antenna element to its internal feeding port, and the active impedance can be found using (9). Therefore, it is efficient to use GTM model to calculate the active impedance with scan angle. Fig. 17 shows the calculated active impedance results of the target element (column 5 and row 5 of the 10×10 array) with scan angle in E-plane.

Once the GTM modules with SBF extraction of array elements are obtained, it is convenient to solve the whole system and predict the performance efficiently with the change of feeding ways of the array elements. The proposed method significantly reduces the computational time and enhances the efficiency of prediction without significant loss of precision.

VI. Conclusion

In this paper, a numerical algorithm is presented to compute the electromagnetic characteristics of large-scale phased antenna array. In this method, the antenna array is divided into

subdomains based on the antenna elements. Each subdomain is described as a GTM module representing the characteristics of internal complex structure and information of the excitation port by an associated GTM and a mapping vector defined on its reference surface. The GTM module of identical structured elements can be reused despite of coordinate translation and rotation operations, and that of the different structured elements can be calculated independently with the parallel scheme. The SBFs of a GTM module in matched situation can be applied in general cases with unmatched terminal load. The GSIE combined with SBF method represents the coupling between modules. For the phased array with fixed element structure and array size, the adjustment of the feeding magnitude and phase does not change the module coupling matrix. Hence, the results of phase and amplitude adjustment can be obtained in a very short period of time, which is the great superiority of the method. The proposed method provides great convenience to predict the performance of large-scale phased antenna array precisely and rapidly.

REFERENCES

[1] R. F. Harrington, *Field Computation by Moment Methods*. New York, NY, USA: Macmillan, 1968.

[2] N. Engheta, W. D. Murphy, V. Rokhlin, and M. S. Vassilion, "The fast multipole method (FMM) for electromagnetic scattering problems," *IEEE Trans. Antennas Propag.*, vol. 40, no. 6, pp. 634–644, Jun. 1992.

[3] J. M. Song and W. C. Chew, "Multilevel fast multipole algorithm for solving combined field integral equations of electromagnetic scattering," *Microw. Opt. Technol. Lett.*, vol. 10, no. 1, pp. 14–19, Sep. 1995.

[4] J. M. Song, C. C. Lu, and W. C. Chew, "MLFMA for electromagnetic scattering from large complex objects," *IEEE Trans. Antennas Propag.*, vol. 45, no. 10, pp. 1488–1493, Oct. 1997.

[5] A. Boag and R. Mittra, "Complex multipole beam approach to electromagnetic scattering problems," *IEEE Trans. Antennas Propag.*, vol. 42, no. 4, pp. 366–372, Apr. 2007.

[6] F. X. Canning, "The impedance matrix localization (IML) method for moment-method calculations," *IEEE Antennas Propag. Mag.*, vol. 42, no. 5, pp. 18–30, Oct. 1990.

[7] E. Bleszynski and T. Jaroszewicz, "AIM: Adaptive integral method for solving large scale electromagnetic scattering and radiation problems," *Radio Sci.*, vol. 31, no. 5, pp. 1225–1251, 1996.

[8] E. Michielssen and A. Boag, "Multilevel evaluation of electromagnetic fields for the rapid solution of scattering problems," *Microw. Opt. Technol. Lett.*, vol. 7, pp. 790–795, Dec. 1994.

[9] S. M. Seo and J.-F. Lee, "A fast IE-FFT algorithm for solving PEC scattering problems," *IEEE Trans. Magn.*, vol. 41, no. 9, pp. 1476–1479, Oct. 1997.

[10] V. Prakash and R. Mittra, "Characteristic basis function method: Anew technique for efficient solution of method of moments matrix equations," *Microw. Opt. Technol. Lett*, vol. 36, pp. 95–100, Jan. 2003.

[11] L. Matekovits, V. A. Laza, and G. Vecchi, "Analysis of large complex structures with the synthetic-functions approach," *IEEE Trans. Antennas Propag.*, vol. 55, no. 9, pp. 2509–2521, Sep. 2007.

[12] W. B. Lu, T. J. Cui, Z. G. Qian, X. X. Yin, and W. Hong, "Accurate analysis of large-scale periodic structures using an efficient sub-entire-domain basis function method," *IEEE Trans. Antennas Propag.*, vol. 52, no. 11, pp. 3078–3085, Nov. 2004.

[13] D. J. Bekers, S. J. L. van Eijndhoven, A. A. F. van de Ven, P. P. Borsboom, and A. G. Tijhuis, "Eigencurrent analysis of resonant behavior in finite antenna arrays," *IEEE Trans. Microw. Theory Tech.*, vol. 54, no. 6, pp. 2821–2829, Jun. 2006.

[14] E. Suter and J. R. Mosig, "A subdomain multilevel approach for the efficient MoM analysis of large planar antennas," *Microw. Opt. Technol. Lett.*, vol. 26, no. 4, pp. 270–277, Aug. 2000.

[15] S. C. Lee, M. N. Vouvakis, and J. F. Lee, "A non-overlapping domain decomposition method with non-matching grids for modeling large finite antenna arrays," *J. Comput. Phys.*, vol. 203, pp. 1–21, Feb. 2005.

[16] Y. Li and J. M. Jin, "A vector dual-primal finite element tearing and interconnecting method for solving 3-D large-scale electromagnetic problems," *IEEE Trans. Antennas Propag.*, vol. 54, no. 10, pp. 3000–3009, Oct. 2006.

[17] V. V. Veremey and R. Mittra, "Domain decomposition approach for capacitance computation of nonorthogonal interconnect structures," *IEEE Trans. Microw. Theory Tech.*, vol. 48, no. 9, pp. 1428–1434, Sep. 2000.

[18] M. K. Li and W. C. Chew, "Wave-field interaction with complex structures using equivalence principle algorithm," *IEEE Trans. Antennas Propag.*, vol. 55, no. 1, pp. 130–138, Jan. 2007.

[19] P. Yla-Oijala and M. Taskinen, "Electromagnetic scattering by large and complex structures with surface equivalence principle algorithm," *Waves Random Complex Media*, vol. 19, pp. 105–125, Feb. 2009.

[20] A. M. van de Water, B. P. de Hon, M. C. van Beurden, A. G. Tijhuis, and P. de Maagt, "Linear embedding via Green's operators: A modeling technique for finite electromagnetic bandgap structures," *Phys. Rev. E*, vol. 72, p. 056704, Nov. 2005.

[21] G. B. Xiao, J. F. Mao, and B. Yuan, "Generalized transition matrix for arbitrarily shaped scatterers or scatterer groups," *IEEE Trans. Antennas Propag.*, vol. 56, no. 12, pp. 3723–3732, Dec. 2008.

[22] G. B. Xiao, J. F. Mao, and B. Yuan, "A generalized surface integral equation formulation for analysis of complex electromagnetic systems," *IEEE Trans. Antennas Propag.*, vol. 57, no. 3, pp. 701–710, Mar. 2009.

[23] W. T. Chen, G. B. Xiao, S. Xiang, and J. F. Mao, "A note on the construction of synthetic basis functions for antenna arrays," *IEEE Trans. Antennas Propag.*, vol. 60, no. 7, pp. 3509–3512, Jul. 2012.

[24] B. Zhang, G. B. Xiao, J. F. Mao, and Y. Wang, "Analyzing large-scale non-periodic arrays with synthetic basis functions," *IEEE Trans. Antennas Propag.*, vol. 58, no. 11, pp. 3576–3584, Nov. 2010.

[25] K. Kurokawa, "Power waves and the scattering matrix," *IEEE Trans. Microw. Theory Tech.*, vol. MTT-13, no. 3, pp. 194–202, Mar. 1965.

[26] A. Safaai-Jazi, "A new formulation for the design of Chebyshev arrays," *IEEE Trans. Antennas Propag.*, vol. 42, no. 3, pp. 439–443, Mar. 1994.

Shang Xiang (S'11) received the B.S. degree in electric engineering from East China Normal University, Shanghai, China, in 2010, and is currently pursuing the Ph.D. degree at the Key Laboratory of Ministry of Education of Design and Electromagnetic Compatibility of High Speed Electronic Systems, Shanghai Jiao Tong University, Shanghai, China.

His research interests are in scattering analysis and computational electromagnetics.

Gaobiao Xiao (M'10) was born in China in 1965. He received the B.S. degree from Huazhong University of Science and Technology, Wuhan, China, in 1988, the M.S. degree from the National University of Defense Technology, Changsha, China, in 1991, and the Ph.D. degree from Chiba University, Chiba, Japan, in 2002, all in electronic engineering.

He joined the Department of Electrical and Electronics Engineering, Hunan University, Changsha, China, as a Research Associate from 1991 to 1997. Since 2004, he has been a Faculty Member with the Department of Electronic Engineering, Shanghai Jiao Tong University, Shanghai, China. His research interests are numerical methods in electromagnetic fields, coupled thermo-electromagnetic analysis, microwave filter designs, fiber-optic filter designs, and inverse scattering problems.

Xuezhe Tian (S'12) received the B.S. degree in electrical and information engineering from Harbin Engineering University, Harbin, China, in 2011, and is currently pursuing the Ph.D. degree in electronic engineering at Shanghai Jiao Tong University, Shanghai, China.

His research interests include computational electromagnetics and its application in scattering and radiation problems.

Junfa Mao (M'92–SM'98–F'12) was born in 1965. He received the B.S. degree in radiation physics from the University of Science and Technology of National Defense, Changsha, China, in 1985, the M.S. degree in experimental nuclear physics from Shanghai Institute of Nuclear Research, Shanghai, China, in 1988, and the Ph.D. degree in electronic engineering from Shanghai Jiao Tong University, Shanghai, China, in 1992.

Since 1992, he has been a faculty member with Shanghai Jiao Tong University, where he is currently a Chair Professor and the Dean of the School of Electronic, Information and Electrical Engineering. He was a Visiting Scholar with the Chinese University of Hong Kong, Hong Kong, from 1994 to 1995, and a Postdoctoral Researcher with the University of California, Berkeley, CA, USA, from 1995 to 1996. He has authored or coauthored more than 190 journal papers (including 90 IEEE journal papers) and 120 international conference papers. His research interests include the interconnect and package problem of integrated circuits and systems and analysis and design of microwave circuits.

Dr. Mao is a Chief Scientist of The National Basic Research Program of China, a project leader of the National Science Foundation for Creative Research Groups of China, a Cheung Kong Scholar of the Ministry of Education, China, an Associate Director of the Microwave Society of China Institute of Electronics, the 2007–2009 Chair of the IEEE Shanghai Section, and the 2009–2013 Chair of IEEE MTT-S Shanghai Chapter. He earned the National Natural Science Award of China in 2004, the National Technology Invention Award of China and the Best Paper Award of APEMC Symposium in 2008, and the National Science and Technology Advancement Award of China in 2012.